Biomedicine & Pharmacotherapy 108 (2018) 670–678

Contents lists available at ScienceDirect

Biomedicine & Pharmacotherapy

journal homepage: www.elsevier.com/locate/biopha

Design, synthesis, *in vitro, in vivo and in silico* pharmacological characterization of antidiabetic *N*-Boc-L-tyrosine-based compounds☆

Miguel Ángel Herrera-Rueda[a], Hugo Tlahuext[b], Paolo Paoli[c], Abraham Giacoman-Martínez[d], Julio César Almanza-Pérez[d], Horacio Pérez-Sánchez[e], Abraham Gutiérrez-Hernández[a], Fabiola Chávez-Silva[a], Elix Alberto Dominguez-Mendoza[a], Samuel Estrada-Soto[a], Gabriel Navarrete-Vazquez[a,*]

[a] *Facultad de Farmacia, Universidad Autónoma del Estado de Morelos, Cuernavaca, Morelos 62209, Mexico*
[b] *Centro de Investigaciones Químicas, Universidad Autónoma del Estado de Morelos, Cuernavaca, Morelos, 62209, Mexico*
[c] *Dipartimento di Scienze Biomediche Sperimentali e Cliniche, Sezione di Scienze Biochimiche, Università degli Studi di Firenze, Viale Morgagni 50, 50134, Firenze, Italy*
[d] *Laboratorio de Farmacologia, Depto. Ciencias de la Salud, Universidad Autónoma Metropolitana-Iztapalapa, México, D.F. 09340, Mexico*
[e] *Bioinformatics and High Performance Computing Research Group (BIO-HPC), Computer Engineering Department, Universidad Católica de Murcia (UCAM), E30107, Murcia, Spain*

ARTICLE INFO

Keywords:
Diabetes
PTP-1B
PPAR
GLUT-4
Polypharmacology
Drug design

ABSTRACT

In this study, we synthesized five *N*-Boc-L-tyrosine-based analogues to glitazars. The *in vitro* effects of compounds **1–5** on protein tyrosine phosphatase 1B (PTP-1B), peroxisome proliferator-activated receptor alpha and gamma (PPARα/γ), glucose transporter type-4 (GLUT-4) and fatty acid transport protein-1 (FATP-1) activation are reported in this paper. Compounds **1** and **3** were the most active in the *in vitro* PTP-1B inhibition assay, showing IC_{50}s of approximately 44 μM. Treatment of adipocytes with compound **1** increased the mRNA expression of PPARγ and GLUT-4 by 8- and 3-fold, respectively. Moreover, both compounds (**1** and **3**) also increased the relative mRNA expression of PPARα (by 8-fold) and FATP-1 (by 15-fold). Molecular docking studies were performed in order to elucidate the polypharmacological binding mode of the most active compounds on these targets. Finally, a murine model of hyperglycemia was used to evaluate the *in vivo* effectiveness of compounds **1** and **3**. We found that both compounds are orally active using an exploratory dose of 100 mg/kg, decreasing the blood glucose concentration in an oral glucose tolerance test and a non-insulin-dependent diabetes mellitus murine model. In conclusion, we demonstrated that both molecules showed strong *in vitro* and *in vivo* effects and can be considered polypharmacological antidiabetic candidates.

1. Introduction

Type 2 diabetes mellitus (T2DM), a chronic metabolic disease, affects the quality of life of individuals worldwide and is characterized by increased blood glucose concentrations (> 120 mg/dL or > 7 mM) caused by a deficiency in insulin production by the pancreas or by the inactivation of some proteins involved in the insulin signaling pathway (insulin resistance) [1,2]. In addition, it is well known that diabetic patients often show high plasma triglyceride concentrations [3,4] which leads to the development atherosclerotic vascular disease, increasing worldwide mortality [5,6]. Currently, experimental T2DM drug discovery is focused on compounds with insulin-sensitizing activity that acts *via* several mechanisms. Some of them are mediated by peroxisome-proliferator activated receptors, which include 3 different subtypes of nuclear receptors: PPARα, PPARγ, and PPARδ [7]. Every isoform controls tissue-specific target proteins that act as lipid sensors. The activation of PPARα reduces triglycerides by increasing fatty acid transport protein-1 (FATP-1) which is expressed in some insulin-sensitive tissues and increases the cellular uptake of long chain fatty acids [8], showing beneficial, preventative effects on cardiovascular risks [9]. Furthermore, PPARγ activation in muscle and adipose tissue causes insulin sensitization by increasing glucose transporter type 4 (GLUT4) expression, which is one of the proteins involved in the insulin signaling pathway [10,11]. Indeed, it has been widely demonstrated that increased translocation and activation of GLUT-4 is essential for increased glucose uptake and improved glucose homeostasis in murine models

☆ Taken in part from the Ph D. thesis of M. A. Herrera-Rueda.

* Corresponding author.
E-mail address: gabriel_navarrete@uaem.mx (G. Navarrete-Vazquez).

https://doi.org/10.1016/j.biopha.2018.09.074
Received 6 June 2018; Received in revised form 12 September 2018; Accepted 12 September 2018
0753-3322/ © 2018 Elsevier Masson SAS. All rights reserved.

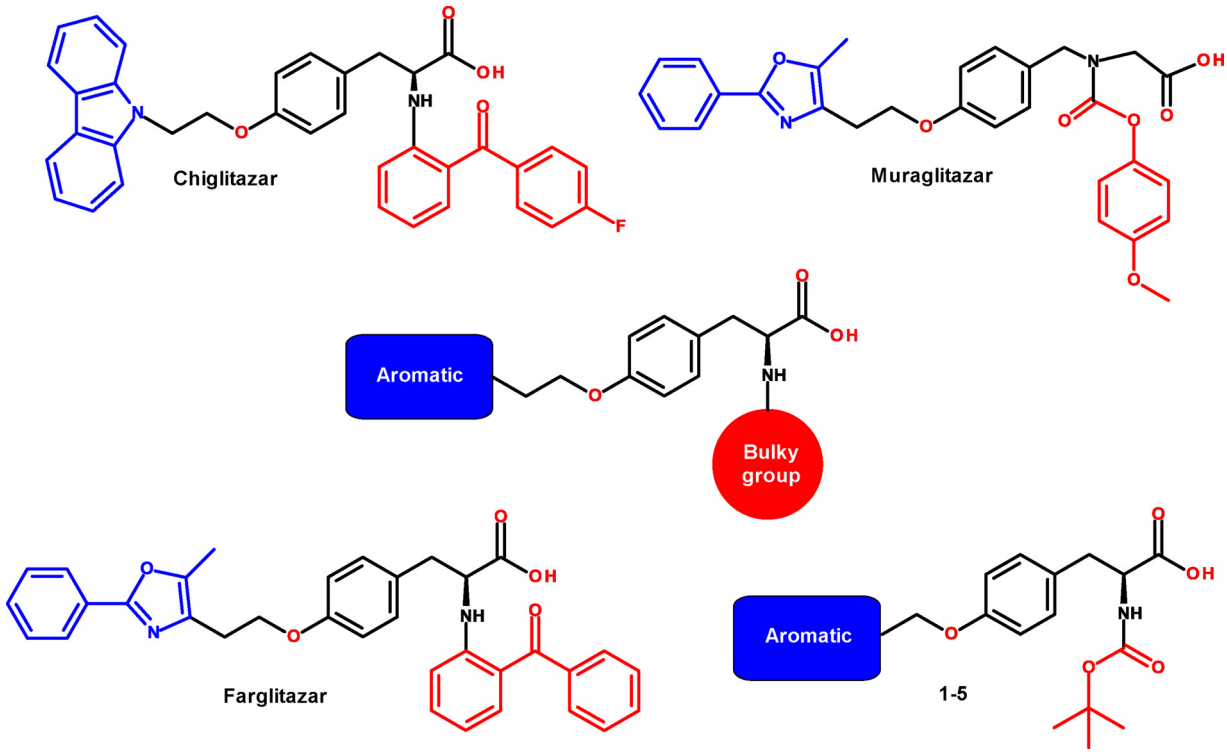

Fig. 1. Unified pharmacophore (center) for glitazars: Chiglitazar, muraglitazar, farglitazar and *N*-Boc-L-tyrosine derivatives **1–5**.

[12]. PPARα and γ are dual agonists based on a tyrosine scaffold belonging to the glitazar family (chiglitazar, farglitazar and muraglitazar; Fig. 1), which was developed to increase insulin sensitivity and simultaneously prevent diabetic cardiovascular complications [9,13–15]. Glitazars have been evaluated in large scale phase III clinical trials in T2DM patients in the last 20 years. Unfortunately, despite being effective at reducing triglycerides, raising HDL levels and improving insulin sensitivity, they also induced severe side effects, forcing researchers to interrupt the development of that kind of molecule [16]. Another promising molecular target for the treatment of diabetes *via* insulin sensitization is protein tyrosine phosphatase 1B (PTP-1B). This intracellular enzyme is involved in down-regulation of receptor tyrosine kinase activity following stimulation of the insulin or leptin receptors [17]. The PTP-1B inhibition causes the insulin receptor to remain in an activated state and hence extends the signaling pathway, thereby improving glucose uptake [18–20]. In addition to known drugs (farglitazar and chiglitazar), other compounds are based on a tyrosine scaffold and have been reported as PPAR α/γ dual agonists [21]. These compounds, which could be beneficial in diabetic cardiomyopathy, possess a unified pharmacophore made up of an acid moiety, a central phenyl ring, linked to an aromatic tail through an aliphatic linker and a bulky group tail connected to the amino group of tyrosine (Fig. 1) [22]. Compounds with dual action as PPARγ activators and PTP-1B inhibitors have been reported elsewhere [23].

From our ongoing research on PPARα and PPARγ dual activators with cardiometabolic activities, we report the design and synthesis of five compounds based on the *N*-Boc-L-tyrosine scaffold (**1–5**) containing the unified glitazar pharmacophore (with the *N*-Boc as the bulky group) along with the *in vitro* relative mRNA expression of PPARα, PPARγ, FATP-1 and GLUT-4. We also describe the inhibition of PTP-1B by these compounds and the molecular docking of the most active compound in the ligand binding site of both PPARs and PTP-1B and its *in vivo* antidiabetic effect using a murine model of hyperglycemia.

2. Materials and methods

2.1. Chemistry

The reagents were purchased from Merck/Sigma-Aldrich (Mexico). The melting point (m.p.) was calculated on an MPA120 EZ-Melt automated apparatus, and the values were not corrected. Thin layer chromatography visualized with UV light and iodine vapors were employed to monitor reactions. Based on respective spectral data, the chemical structures of the prepared molecules were confirmed. ^{1}H and ^{13}C NMR studies were conducted on Varian Oxford (400 MHz) and (100 MHz) instruments, respectively. Chemical shifts and coupling constants are given in ppm and Hz. Infrared (IR) spectra were obtained from a Bruker Vector 22 FT spectrophotometer. High Resolution Mass Spectrometry (HRMS) was performed with JEOL JMS-700 equipment. Optical rotations were measured by Perkin Elmer model 241 polarimeter at room temperature (20 °C) and 589 nm (concentration in 0.01 g/1 mL $CHCl_3$).

2.1.1. General preparation of **1–5**

A solution of *N*-(*tert*-butoxycarbonyl)-L-tyrosine (**13**) (0.2 g, 0.6 mmol) in CH_3CN (4 mL) was reacted with potassium carbonate (0.327 g, 2.3 mmol, 3.5 eq.). After the reaction mixture was stirred at room temperature for 30 min, adequately substituted methylarylhalides (**6–10**) were added (0.6 mmol, 1 eq.). The reaction was stirred at 70 °C for 9 h. The reaction was monitored by thin layer chromatography. After complete conversion, solvent was extracted in vacuum and 2 mL of cold water was added to the residue, and an acidic pH was reached with dilute HCL solution (10%). The aqueous layer was extracted, and the organic solvent was evaporated in vacuum. All compounds were purified by Preparative Layer Plates (PLC), and silica was extracted with CH_2Cl_2; the solvent was filtered and evaporated in vacuum obtaining a pure solid.

2.1.1.1. (R)-3-(4-((1H-benzo[d]imidazol-2-yl)methoxy)phenyl)-2-((tert-butoxycarbonyl)amino) propanoic acid (1). Yellow crystals were obtained with 89% yield. M.p. 113.7–114.2 °C. $[\alpha]_{20}^{D}$ + 2 (c, 0.1,

$CHCl_3$). IR (cm^{-1}): 1018 **(C—O—C)**, 1244 **($C(CH_3)_3$)**, 1510 **(N=C)**, 1612 **(NCOO)**, 1685 **(COO)**. ^{1}H NMR (400 MHz, DMSO-*d6*) δ:1.26 (s, 9H, **CH_3**), 2.85 (m, 2H, **Hβ**), 3.8 (b, 1H, **Hα**), 4.67 (s, 2H, **OCH_2**), 6.56 (d, *Jo* = 8.2 Hz, 2H, **H3, H5**), 6.89 (d, *Jo* = 8.2 Hz, 2H, **H2, H6**), 7.12 (dd, *Jo* = 9.2, 3.4 Hz, 2H, **H5′**, **H6′**) 7.48 (dd, *Jo* = 9.0, 3.0 Hz, 2H, **H4′**, **H7′**), ppm. ^{13}C NMR (100 MHz, DMSO-d_6) *δ*: 28.59 (**CH_3**), 37.17 (**Cβ**), 57.12 (**Cα**), 57.82 (**OCH_2**), 78.08 (**C-*tert***), 115.14 (**C3, C5**), 115.27 (**C4′,C7′**), 122.04 (**C5′,C6′**), 129.33 (**C1**), 130.69 (**C2, C6**), 138.72 (**C3′a, C7a'**), 155.29 (**C2′**), 155.86 (**NCOO**), 155.96 (**C4**), 175.39 (**COOH**) ppm; H.R.M.S.(FAB $^+$): *m/z* 412.1899 $[M+H]^+$ (calculated for $C_{22}H_{25}N_3O_5H^+$ 412.1794).

*2.1.1.2. (R)-2-((tert-butoxycarbonyl)amino)-3-(4-(quinolin-2-ylmethoxy) phenyl)propanoic acid (**2**)*. White crystals were obtained with 87% yield. M.p. 139.8–140.0 °C. $[\alpha]_{20}^{D}$ + 14 (*c*, 0.1, $CHCl_3$). IR (cm^{-1}): 1020–1161 **(C—O—C)**, 1243 **($C(CH_3)_3$)**, 1508 **(N=C)**, 1611 **(NCOO)**, 1705 **(COO)**.^{1}H NMR (400 MHz, DMSO-d_6) δ: 1.41 (s, 9H, **CH_3**), 3.12 (m, 2H, **Hβ**), 4.60 (b, 1H, **Hα**), 5.23 (s, 2H, **OCH_2**) 6.86 (d, *Jo* = 7.6 Hz, 2H, **H3, H5**), 7.14 (d, *Jo* = 7.6 Hz, 2H, **H2, H6**), 7.52 (t, *Jo* = 7.2 Hz, 1H, **H3′**), 7.70 (t, *Jo* = 8.4 Hz, 2H, **H6′**), 7.70 (t, *Jo* = 7.2 Hz, 2H, **H7′**), 7.79 (d, *Jo* = 7.76 Hz, 1H, **H5′**), 7.79 (d, *Jo* = 7.76 Hz, 1H, **H5′**), 8.12 (d, *Jo* = 8.8 Hz, 1H, **H8′**) 8.20 (d, *Jo* = 8.12 Hz, 1H, **H4′**) ppm. ^{13}C NMR (100 MHz, DMSOd6) *δ*: 28.55 (**CH_3**), 37.45 (**Cβ**), 54.74 (**Cα**), 69.74 (**OCH_2**), 80.02 (**C*tert***), 114.89 (**C3, C5**), 119.34 (**C3″**), 127.12 (**C6″**), 127.51 (**C5″**), 127.85 (**C4″a**), 127.97 (**C1**), 129.49 (**C7″**), 130.69 (**C8″**), 130.94 (**C2, C6**), 138.51 (**C4″**), 146.28 (**C8″a**), 155.53 (**C4**), 157.32 (**C2″**), 158.11 (**NCOO**), 174.51 (**COO**) ppm; H.R.M.S.(FAB $^+$): *m/z* 423.1911 $(M+H)^+$ (Calculated for $C_{24}H_{26}N_2O_5H^+$ 423.1842).

*2.1.1.3. (R)-2-((tert-butoxycarbonyl)amino)-3-(4-((2′-cyano-[1,1′-biphenyl]-4-yl)methoxy) phenyl)propanoic acid (**3**)*. White crystals obtained with 92% yield. M.p. 133.5–135.3 °C. $[\alpha]_{20}^{D}$ + 9 (*c*, 0.1, $CHCl_3$). IR (cm^{-1}): 1005–1210 **(C—O—C)**, 1243 **($C(CH_3)_3$)**, 1510–1533 **(C=C)**, 1594 **(NCOO)**, 1666 **(COO)**, 2222 **(Ar-CN)**. ^{1}H NMR (400 MHz, $CDCl_3$) δ: 1.33 (s, 9H, **CH_3**), 2.93 (m, 2H, **Hβ**), 4.23 (d, 1H, **Hα**), 5.16 (s, 2H, **OCH_2**), 6.96 (d, *Jo* = 6.8 Hz, 2H, **H3, H5**), 7.19 (d, *Jo* = 7.2 Hz, 2H, **H2, H6**), 7.43 (d, *Jo* = 7.2 Hz, 1H, **H4″**), 7.57 (m, 5H, **H2′**, **H3′**, **H5′**, **H6′** **H6″**), 7.76 (d, *Jo* = 5.2 Hz, 1H, **H5″**) 7.93 (d, *Jo* = 6.0 Hz, 1H, **H3″**), ppm. ^{13}C NMR (100 MHz, DMSO-d_6) *δ*: 28.14 (**CH_3**), 35.65 (**Cβ**), 55.79 (**Cα**), 68.73 (**OCH_2**), 78.39 (**C-*tert***), 110.17 (**C2″**) 114.54 (**C3, C5**), 118.60 (**CN**), 127.93 (**C4″**), 128.16 (**C3′, C5′**), 128.76 (**C2′, C6′**), 129.67 (**C1**), 130.20 (**C2, C6**), 133.56 (**C6″**), 133.89 (**C5″**), 136.52 (**C3″**), 137.27 (**C4′**), 137.83 (**C1′**), 144.20 (**C1″**), 157.10 (**NCOO**), 155.52 (**C4**), 172.19 (**COO**) ppm; MS (FAB+) *m/z* 43, 57, 136, 192, 299, 373, 417(M $+H)^+$.

*2.1.1.4. (R)-2-((tert-butoxycarbonyl)amino)-3-(4-(naphthalen-1-ylmethoxy)phenyl)propanoic acid (**4**)*. White crystals were obtained with 85% yield. M.p. 119.6–120.8 °C. $[\alpha]_{20}^{D}$ + 25 (*c*, 0.1, $CHCl_3$). IR (cm^{-1}): 1011–1160 **(C—O—C)**, 1234 **($C(CH_3)_3$)**, 1509–1584 **(C=C)**, 1610 **(NCOO)**, 1705 **(COO)**. ^{1}H NMR (400 MHz, $CDCl_3$) δ: 1.42 (s, 9H, **CH_3**), 3.12 (dd, 2H, **Hβ**), 4.60 (d, 1H, **Hα**), 5.46 (s, 2H, **OCH_2**), 6.97 (d, *Jo* = 8.2 Hz, 2H, **H3, H5**), 7.17 (d, *Jo* = 8.6 Hz, 2H, **H2, H6**), 7.42 (m, *Jo* = 7.0 Hz, 4H, **H3′**), 7.45 (m, *Jo* = 7.8 Hz, 4H, **H2′**), 7.50 (m, *Jo* = 7.2 Hz, 4H, **H6′**), 7.55 (m, *Jo* = 7.8 Hz, 4H, **H7′**), 7.84 (m, *Jo* = 7.8 Hz, 1H, **H4′**), 7.88 (m, *Jo* = 9.2 Hz, 1H, **H-5′**), 8.02 (m, *Jo* = 9.0, 8.0 Hz, 4H, **H8′**) ppm. ^{13}C NMR (100 MHz, CDCl3) *δ*: 28.30 (**CH_3**), 37.01 (**Cβ**), 54.44 (**Cα**), 68.64 (**OCH_2**), 80.29 (**C-*tert***), 115.00 (**C3, C5**), 123.72 (**C8′**), 125.30 (**C2′**), 125.90 (**C6′**), 126.45 (**C7′**), 126.64 (**C3′**), 128.28, (**C1**), 128.67 (**C5′**), 129.02 (**C4′**), 130.52 (**C2, C6**), 131.53 (**C8′a**), 132.24 (**C4′a**), 133.77 (**C1′**), 155.50 (**C4**), 157.99 (**NCOO**), 176.46 (**COO**) ppm; H.R.M.S.(FAB $^+$): *m/z* 421.1862 $[M+H]^+$ (Calculatedd for $C_{24}H_{26}N_2O_5$ 421.1889).

*2.1.1.5. (R)-3-(4-([1,1′-biphenyl]-3-ylmethoxy)phenyl)-2-((tert-butoxycarbonyl)amino)propanoic acid (**5**)*. White crystals were obtained with 92% yield. M.p. 172.2–173.3 °C. $[\alpha]_{20}^{D}$ + 38 (*c*, 0.1, $CHCl_3$). IR (cm^{-1}): 1023–1160 **(C—O—C)**, 1238 **($C(CH_3)_3$)**, 1509–1584 **(C=C)**, 1610 **(NCOO)**, 1708 **(C=O)**. 1H NMR (400 MHz, $CDCl_3$) δ: 1.46 (s, 9H, **CH_3**), 3.15 (m, 2H, **Hβ**), 4.62 (m, 1H, **Hα**), 5.09 (s, 2H, **OCH_2**), 6.97 (d, *Jo* = 8.6 Hz, 2H, **H3, H5**), 7.17 (d, *Jo* = 8.2 Hz, 2H, **H2, H6**), 7.41 (d, *Jo* = 8.6 Hz, 1H, **H6′**), 7.46 (dd, *Jo* = 8.6 Hz, 2H, **H3″**, **H5″**), 7.56 (s, 9H, **H2′**, H**4′**, H**5′**, H**4″**), 7.77 (d, *Jo* = 7.4 Hz, 2H, **H2″**, **H6″**) ppm. ^{13}C NMR (100 MHz, DMSO-d_6) *δ*: 28.36 (**CH_3**), 37.06 (**Cβ**), 54.58 (**Cα**), 70.04 (**OCH_2**), 80.28 (**C-*tert***), 115.00 (**C3, C5**), 126.33 (**C5′**), 126.46 (**C2′**), 126.83 (**C4′**), 127.24 (**C2″, C6″**), 127.47 (**C4″**), 128.85 (**C3″, C5″**), 129.08 (**C1**), 129.08 (**C6′**), 130.56 (**C2, C6**), 137.59 (**C1′**), 140.91 (**C1″**), 141.59 (**C3′**), 155.63 (**C4**), 157.93 (**NCOO**), 175.91 (**COO**) ppm; H.R.M.S.(FAB $^+$): *m/z* 447.1930 $[M+H]^+$ (Calculated for $C_{27}H_{29}NO_5$ 447.2046).

*2.1.2. Preparation of N-(tert-butoxycarbonyl)-L-tyrosine (N-Boc-L-tyrosine, **13**)*

A suspension of L-tyrosine hydrochloride (**12**) (5 g, 22.9 mmol), Boc_2O (15 g, 68.7 mmol, 3 eq) and Et_3N (4.63 g, 45.8 mmol, 2 eq) in CH_2Cl_2 (50 mL) was heated at reflux for 2–3 h. After cooling the mixture to room temperature, a 10% aqueous solution of HCl (10 mL) was added. The layers were separated and the aqueous layer was extracted with $CHCl_3$ (20 mL). The combined organic layers were dried with sodium sulfate and filtered and the solvent evaporated under reduced pressure. The residue was recrystallized from ethanol, yielding 89%. $[\alpha]_{20}^{D}$ + 3.0 (*c*, 0.1, $CHCl_3$), M.p. 133–135 °C.

2.2. Pharmacological evaluation

2.2.1. In vitro PTP-1B studies

PTP-1B complete coding sequence was cloned with the sequence of the glutathione S-transferase (GST) in the pGEX-2 T bacterial expression vector. The *E. coli* TB1 strain was employed for enzyme expression and purification. The recombinant fusion proteins were purified by affinity chromatography on glutathione-Sepharose, treated with thrombin and purified by gel filtration.

2.2.1.1. Phosphatase assay inhibition. The phosphatase assay was carried out at 37 °C using 4-nitrophenylphosphate as substrate. The assay buffer (pH 7.0) contained β,β-dimethylglutarate, EDTA and dithiothreitol. Furthermore, the reactions were started by adding aliquots of the PTP-1B preparation and stopped at proper times by addition of KOH. The amount of 4-nitrophenolate ion released was detected by reading the absorbance of samples at 400 nm (e = 18,000 $M^{-1}\,cm^{-1}$). For each inhibitor, the IC_{50} was calculated by determining the initial hydrolysis rate under a fixed 4-nitrophenylphosphate concentration, equal to the *K*m value, in the presence of increasing inhibitor concentrations. Data obtained were fitted to the following equation using the Fig-Sys software:

$$y = \frac{\text{Max}-\text{Min}}{1+\left(\frac{x}{IC_{50}}\right)^{slope}} + \text{Min}$$

where $y = V_i / V_0$ represents the ratio between the activity measured in the presence of the inhibitor and the activity of enzyme in the absence of inhibitor. The concentration of the inhibitor is represented by the "x" parameter [24]. *K*i values were determined using suitable equations depending on the inhibition mechanisms of the compounds. All initial rates were measured in triplicate [18–20].

2.2.2. In vitro PPAR α/γ, FATP-1 and GLUT-4 assays

Assays were performed as described previously [2,7,25–28]. 3T3-L1 cells (9×10^5 murine fibroblast/well) were cultured using Dulbecco's modified Eagle's medium. Cell viability, following treatment with compounds **1** and **3**, was measured using the 3-(4,5-dimethylthiazole-2-yl)-2,5-diphenyltetrazolium bromide (MTT) assay at different

concentrations ranging from 1 μM to 100 μM. Confluent cultures of **3T3-L1** cells were induced to differentiate to the adipocyte phenotype using 3-isobutyl-1-methylxanthine (0.5 mM), dexamethasone acetate (0.25 μM), and murine insulin (0.8 μM) for 48 h, followed by another insulin pulse. The differentiated cells were treated for 24 h to determine the effects of compounds **1** and **3** at 10 μM on PPARs, FATP1 and GLUT-4 mRNA expression. RNA was isolated from the differentiated cells, and 2 μg of total RNA was reverse-transcribed. Transcriptase was inactivated, and the samples were cooled. For the amplification of every reverse-transcribed reaction, SYB(R)-Green master mix containing 0.5 mM of customized primers for PPARα, PPARγ, GLUT-4, and FATP-1 was used. Polymerase chain reaction (PCR) was employed for each sample measuring the threshold cycles (Ct) and the ΔCt values. Changes in the relative expression levels of each specific gene (ΔΔCt) were calculated [2].

2.2.3. In vivo antidiabetic assay

The experiment was carried out in accordance with the Mexican Federal Regulations for Animal Experimentation and Care (NOM-062-ZOO-1999, SAGARPA), founded on U.S. NIH Publication No. 85-23. CD1 mice weighing 25–30 g were maintained in groups of 6 under laboratory environments with water *ad libitum* and fasted for 16 h. The experimental diabetes model was induced in these mice using a single administration of streptozotocin (STZ, 100 mg/kg, i.p.) 15 min before the injection of nicotinamide (NA, 40 mg/kg, i.p.). The hyperglycemic effect was established as higher glycemic levels (> 180 mg/dL), and animals were designated for the assay. The hyperglycemic mice were divided into 3 groups of 6 animals each (n = 6). Individuals of experimental groups were orally administered a suspension of 100 mg/kg of **1** and **3** in 10% tween 80 (vehicle). The control group was treated only with vehicle. A dose of 5 mg/kg of sulfonylurea (glibenclamide) was employed as a hypoglycemic reference. Samples of mice blood were collected from the caudal veins at 0, 1, 3, 5 and 7 h after oral gavage of compounds **1** and **3**. Blood glucose concentrations were calculated using the Accu-Chek commercial glucometer from Roche. The percent variation of glycemia was calculated using the following formula: %Variation of glycemia = $[(G_x\text{-}G_0)/G_0] \times 100$, where G_0 is initial glycemia level and G_x is the glycemia level at each time point [2,19,20].

2.2.4. Oral glucose tolerance test

Normal glycemic mice were separated into 3 groups of six mice. 30 min after administration of compounds **1** and **3**, a single gavage of glucose solution (2 g/kg) was given to each mouse. Blood samples were obtained as described above at 0, 0.5, 1, 1.5, 2 and 3 h after the oral gavage of vehicle, glibenclamide or a test compound. Plasmatic glucose levels and the percent variation of glycemia for each group were established as mentioned above [29].

2.2.5. Statistical analysis

For *in vivo* experiments (6 mice/group), all values are expressed as the mean ± S.E.M. To analyze the changes in the percent variation of glycemia, ANOVA was used, followed by a Bonferroni test. The *in vitro* studies were carried out in quadruplicate or sextuplicate in Adipocytes or PTP-1B. The statistical analysis for these experiments was an ANOVA complemented with a Dunnett's multiple comparison test. $p < 0.05$ was considered statistically significant. GraphPad Prism 5.0 was employed for data analysis.

2.3. Molecular docking calculation

Crystal structure information of PPARα, PPARγ and PTP-1B was obtained from the Protein Data Bank (PDB) searching the respective PDB codes: 1K7L (resolution: 2.5 Å), 1K74 (2.3 Å) and 4Y14 (1.898 Å). The docking experiments were performed using AutoDock (version 4.2.6.) to execute several runs in each calculation and provide putative binding modes. All molecules of water and the cocrystal ligands were extracted from the crystallographic coordinates. After the docking calculation was finished, the complete solutions were clustered into groups with RMSD < 2.0 Å. MOE 2018.01 [30] and Pymol 1.7.4. were employed for adequate visualization.

2.3.1. Validation of docking experiments

All protocols were validated *via* redocking of cocrystal molecules into the ligand site of each receptor or enzyme target: PPARα (GW409544), PPARγ (GW409544) and PTP-1B (CPT157633). The RMSD between the cocrystal molecule and the performed experiment must be < 2.0 Å in all cases (0.37, 1.23 and 1.87 Å, respectively). These values indicate that the parameters used for calculations agree by replicating the conformation and orientation in the X-ray coordinates of the receptors and enzyme.

3. Results and discussion

3.1. Chemistry

L-tyrosine (**11**) was treated with di-*tert*-butyl dicarbonate (Boc_2O, **12**) to give *N*-Boc-L-tyrosine (**13**). Compounds **1–5** were obtained *via* Williamson synthesis from the reaction of **13** and the appropriately substituted methylarylhalides **6–10** using nonprotic polar solvents and K_2CO_3 as a nonnucleophilic base (Scheme 1). The compounds were recuperated with 85–92% yield, and the purification was done using Preparative Layer Plates (PLC). The chemical structures of the synthesized molecules were confirmed based on their spectral data (NMR and Mass spectra). In the nuclear magnetic resonance experiments (^{1}H NMR; δ ppm), the signals of each proton of the compounds were confirmed based on their chemical shifts, multiplicities, and coupling constants. The five compounds showed a single signal integrated for the 9 hydrogens, ranging from δ_H 1.26 to 1.46 ppm, of the $(CH_3)_3$ of the *N*-Boc group. In all compounds, the aliphatic signals were found at upfield shifts in 3.79 to 4.62 ppm accredited to Hα, and signals ranging from δ 2.85 to 3.15 ppm were assigned to Hβ.The displacements for the methyleneoxy group were found in δ_H 4.67–5.46 ppm (singlet). The aromatic part of the ^{1}H NMR spectra of all compounds possessed an A_2B_2 spin system signals oscillating from δ_H 6.89 to 7.19 ppm (d, J_{ortho} = 6.8–8.6 Hz) and 6.56–6.97 ppm (d, J_{ortho} = 7.2–8.6 Hz) accredited to the equivalent hydrogens (H-2′, H-6′ and H-3′, H-5′, respectively) of the phenyl-*p*-substituted tyrosine scaffold. In the ^{13}C NMR spectra, persistent signals were found for the *N*-Boc-L-tyrosine scaffold: One signal fluctuated from δ_C 28.1 to 28.6 ppm, attributed to the $(CH_3)_3$ of the *N*-Boc group; two signals oscillated from δ_C 54.4 to 57.1 and 35.6 to 37.4 ppm, attributed to α and β aliphatic carbons, respectively.

An additional recurrent signal associated with the CH_2O group was located in upfield shifts fluctuating from δ_C 57.8 to 70.0 ppm. A constant signal appeared in δ_C 78.1 to 80.3 ppm, attributed to C-*tert* of *N*-Boc group. In the aromatic region, four persistent signals were found: 127.9 to 129.7 (C-1), 130.1 to 130.7 (C-2 and C-6), 114.5 to 115.1 (C-3 and C-5) and 155.5 to 155.9 (C-4) ppm, corresponding to the benzene nucleus of tyrosine. Another two frequent signals were located in downfield shifts from δ_C 155.9 to 157.9 ppm given to C═O group belonging to *N*-Boc as well as the COOH signal found in δ_C 172.2–176.5 ppm.

3.2. The in vitro PTP-1B assay

The results of preliminary enzymatic assays carried out by using a fixed inhibitor concentration (final concentration was 50 μM) are reported in Fig. 2. We observed that compound **1** (with benzimidazole substituent) and compound **3** (with biphenylcarbonitrile substituent) inhibit the activity of PTP-1B by 60% and 80%, respectively, compared with the control test (0% of inhibition). In contrast, compounds **2** (quinolinyl), **4** (naphthyl) and **5** (*m*-biphenyl) behave as weaker

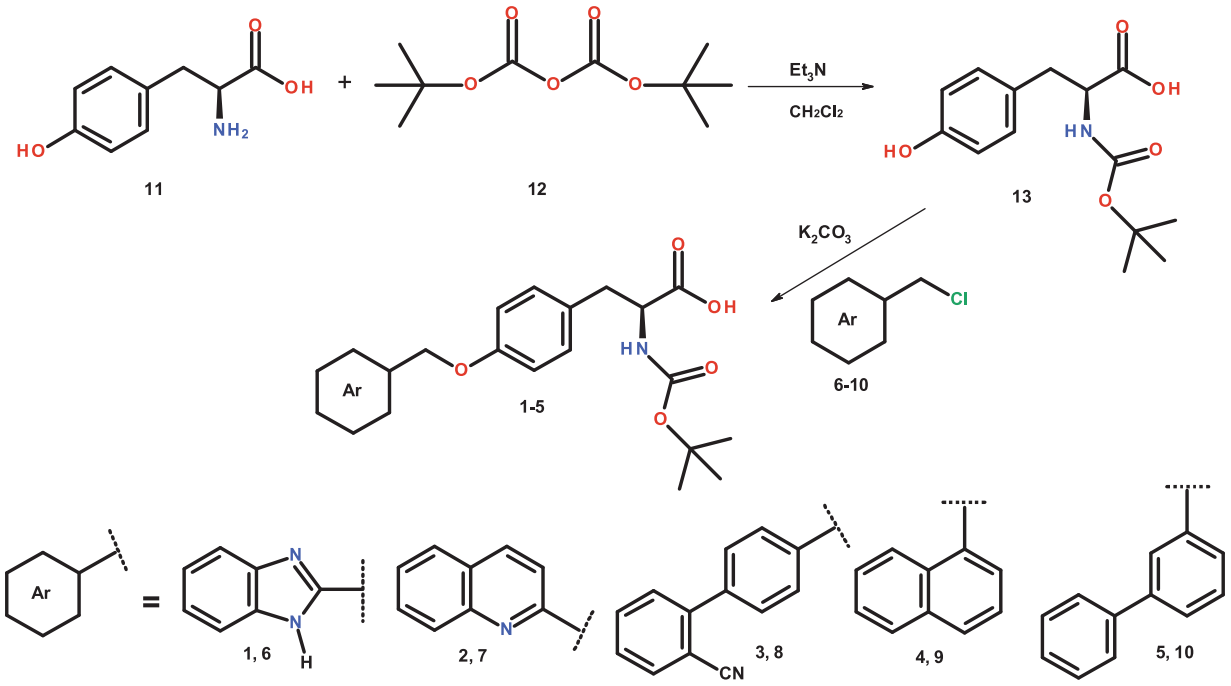

Scheme 1. Synthetic scheme of compounds **1–5**.

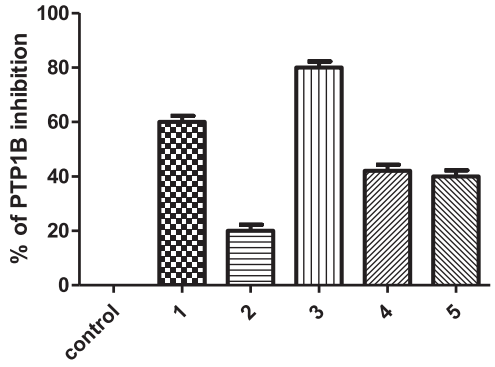

Fig. 2. Percentage of inhibition of PTP-1B activity obtained by incubating the enzyme in the presence of compounds **1–5** at 50 μM. DMSO was used as the control. Each bar represents the mean ± S.E.M. (n = 4).

inhibitors.

Taking these results into account, an additional test was performed to calculate the IC_{50} for the most active inhibitors, namely, compounds **1** and **3**. For this purpose, we studied the PTP-1B catalyzed hydrolysis of 4-nitrophenyl phosphate by using different concentrations of compounds **1** and **3** calculating the time-course of 4-nitrophenol releasing (measured at 400 nm). The initial rates decreased with cumulative inhibitor concentrations; thereby, the IC_{50}s were determined (Fig. 3). We found that the two compounds are equipotent because they showed IC_{50}s of 43.6 ± 0.7 and 44 ± 3.0 μM, respectively.

To obtain compounds with polypharmacological activities and to continue with the *in vitro* tests on PPARα/γ, an initial screening was carried out selecting only compounds **1** and **3** as the best candidates since they were the most potent and selective as PTP-1B inhibitors.

3.3. Relative expression of PPARs, FATP-1 and GLUT-4

Fibroblasts were differentiated to the adipocytes to determine the influence of testing molecules on PPARα, PPARγ, GLUT-4 and FATP-1 expression. Differentiated cells were treated for 24 h with 10 μM of molecules **1, 3,** fenofibrate (FEN) and pioglitazone (PIO), both used as reference drugs. Then, changes in the mRNA expression levels were calculated. Figs. 4 and 5 show that these compounds significantly increased the levels of PPARs, FATP-1 and GLUT-4 mRNA expression to a greater extent than fenofibrate and pioglitazone.

Compound **1** significantly increased the relative mRNA expression levels of PPARα (approximately 8-fold) and its downstream gene FATP-1 (10-fold). This activation of PPARα by compound **1** could reduce triglycerides by increasing FATP-1 which could enhance the cellular uptake of fatty acids and lead to beneficial preventative effects on cardiovascular risks. FATP-1 also plays an important role in the incorporation of postprandial fatty acids into adipose tissue and muscle as well as in the etiology of diet-induced insulin resistance and metabolic disease [8]. Compound **3** also increased the levels of mRNA expression of PPARα (approximately 3-fold) and FATP-1 (15-fold).

On the other hand, compound **1** significantly increased the mRNA levels of PPARγ (approximately 8-fold) and its downstream gene GLUT-4 (2.5-fold). Activation of PPARγ may reduce glycemia in diabetic people *via* insulin sensitization. Multiple line of evidence specify that increased GLUT-4 in skeletal muscle is essential for glucose control [2], and these results suggest that compound **1** induces GLUT-4 mRNA expression to a greater extent than pioglitazone.

Moreover, compound **3** did not induce a meaningful increase in the mRNA expression levels of PPARγ or GLUT-4. These results indicate that an increase in the expression of the downstream genes FATP-1/GLUT4 is not always dependent upon high mRNA expression of PPARα/γ. Finally, it was clearly observed that compound **1** possesses polypharmacological activities by increasing the mRNA expression of PPARα, PPARγ and their downstream genes (FATP-1 and GLUT-4, respectively). Therefore, it could decrease plasma glucose and triglycerides levels, increase insulin sensitivity and simultaneously prevent cardiovascular complications. Polypharmacological (multitarget) activity is the modulation of different molecular targets to reach a desired therapeutic effect [2]. It refers to molecules that are recognized by different drug targets [31]. A polypharmacological treatment that regulates glucose levels and diminished several complications related to hyperglycemia and insulin resistance would be an attractive choice for T2DM therapy.

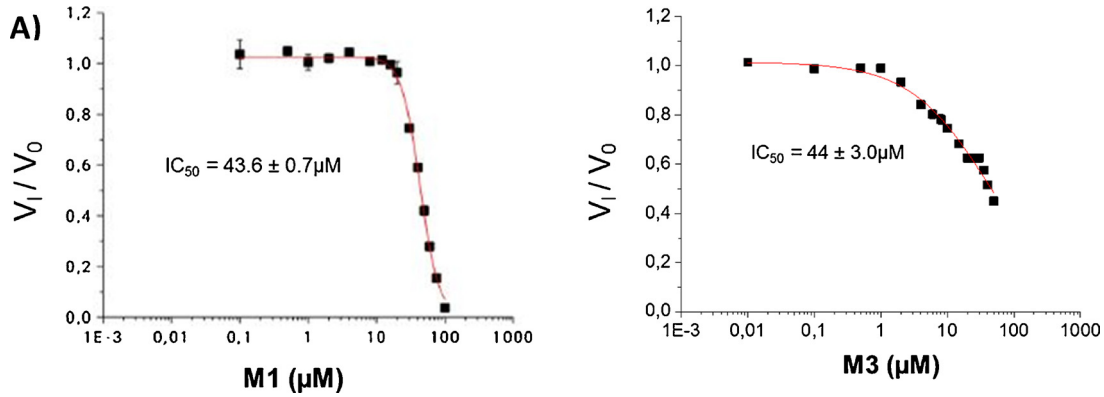

Fig. 3. The IC_{50} for compounds **1** (A) and **3** (B) was calculated by plotting the data for the residual activity of PTP-1B against the concentration of compounds **1** and **3**. Fifteen inhibitor concentrations were employed. All assays were conducted in quadruplicate. Data represent the mean ± S.E.M.

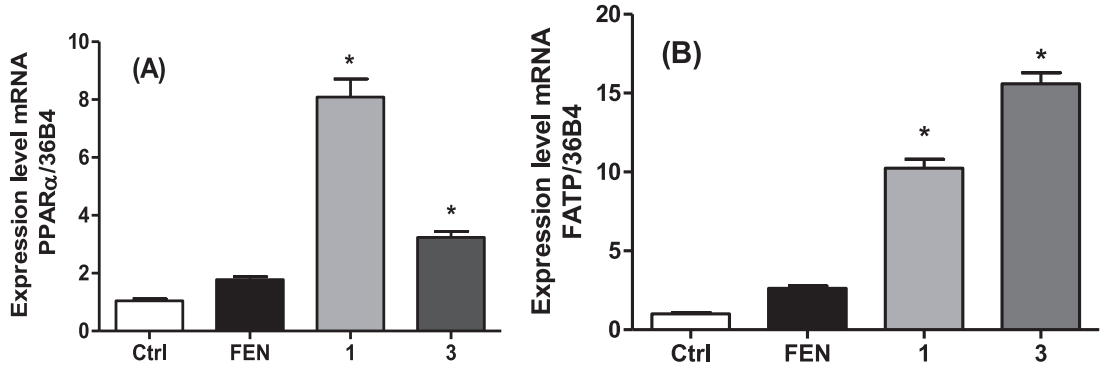

Fig. 4. (A) Influence of **1**, **3** and fenofibrate on changes in the relative mRNA expression of PPARα. (B) Influence of **1**, **3** and fenofibrate on the relative mRNA expression of FATP-1. Results are means ± S.E.M. (n = 5). *p < 0.001 compared with the control group.

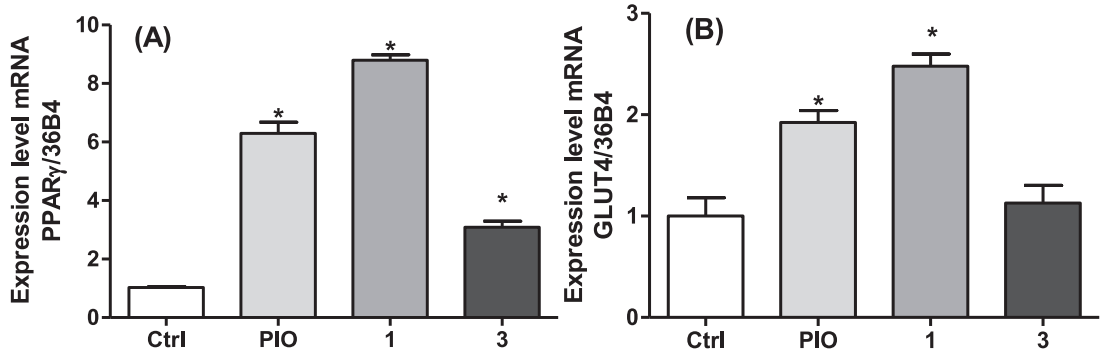

Fig. 5. (A) Influence of **1**, **3** and pioglitazone on the relative mRNA expression of PPARγ. (B) Influence of **1**, **3** and pioglitazone on the relative mRNA expression of GLUT-4. Results are means ± S.E.M. (n = 5). p < 0.001 compared with the control group.

3.4. In vivo assays

3.4.1. Antidiabetic activity of compounds 1 and 3

Compounds **1** and **3** were the most potent for the three T2DM protein targets selected, and both were chosen to evaluate their *in vivo* effects on STZ/NA diabetic mice, an experimental non-insulin-dependent diabetes murine model [2,7,25]. As a hypoglycemic control, glibenclamide was employed to confirm that the pancreas damage induced in this model was limited and that the pancreatic β-cells still generated insulin responding to the secretagogue signal. Compounds **1** and **3** were administered *via* intragastric gavage using an experimental dose of 50 mg/kg. Administration of compounds **1** and **3** significantly decreased plasma glucose concentration ($p < 0.05$) during acute time periods (7 h) compared with the vehicle group (Fig. 6). Compound **1** showed the best activity, decreasing blood glucose levels after the first hour, compared with compound **3** which started decreasing glucose levels after three hours. The pharmacodynamic and pharmacokinetic behavior of compound **1** could be attributed to the benzimidazole-privileged structure in the hydrophobic region of the *N*-Boc-L-tyrosine derivatives generating a continued decrease in glycemia, by nearly 50% at 7 h after compound oral administration. Compound **3** reduced glycemia three hours after intragastric gavage (−20% at 3 h and −45% at 5 h). Moreover, a statistically significant difference was observed between **3** and the vehicle group at the end of the experiment, when the maximum influence of the compound was obtained (Fig. 6).

3.4.2. Oral glucose tolerance test (OGTT) in normoglycemic mice

To verify the plausible antihyperglycemic or hypoglycemic effect of compounds, we carried out an oral glucose tolerance test in normoglycemic mice. Compounds **1** and **3** were chosen according to the

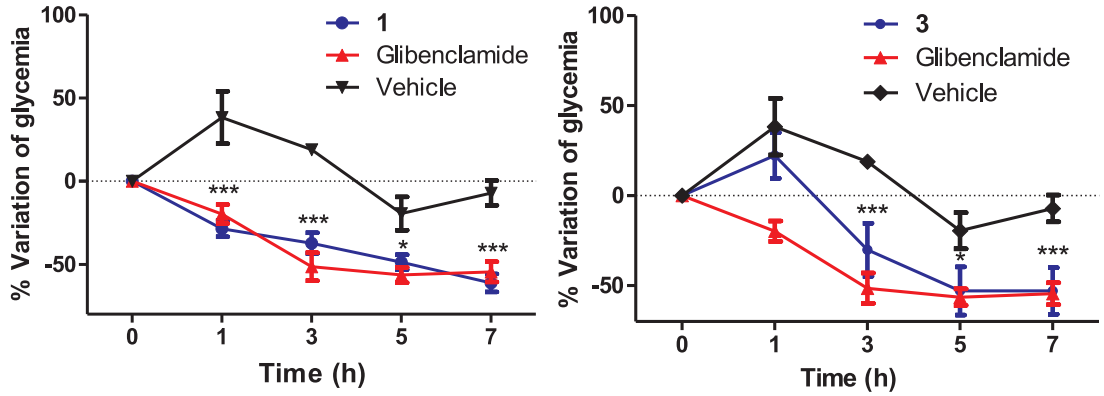

Fig. 6. Influence of an intragastric 100 mg/kg dose of compound **1** or **3** or 5 mg/kg glibenclamide in the STZ/NA hyperglycemic mouse model (n = 6). ***p < 0.05 *versus* the vehicle group (Tween 80, 10% v/v).

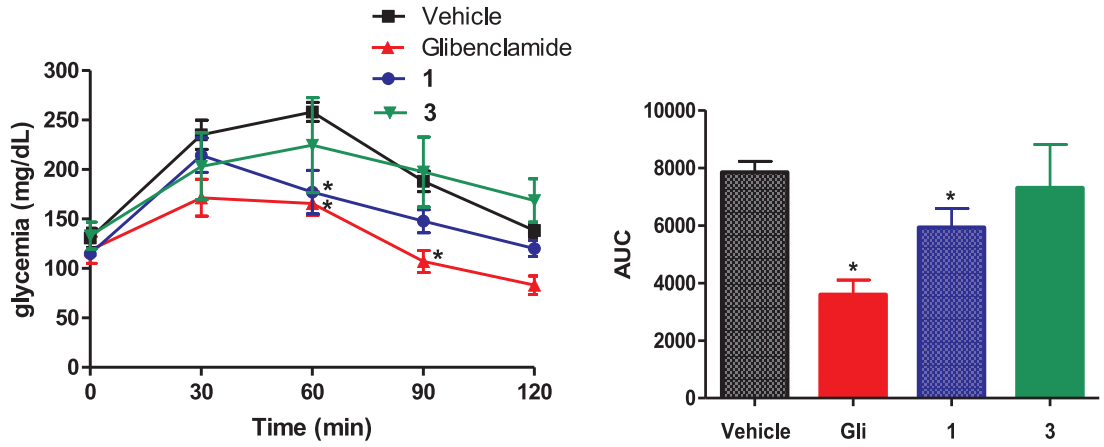

Fig. 7. (A) OGTT and B) AUC of compounds **1** and **3.** *Significantly different from the vehicle group. One-way and two-way ANOVA with post hoc Dunnett's test (n = 6, mean ± SEM, p < 0.05).

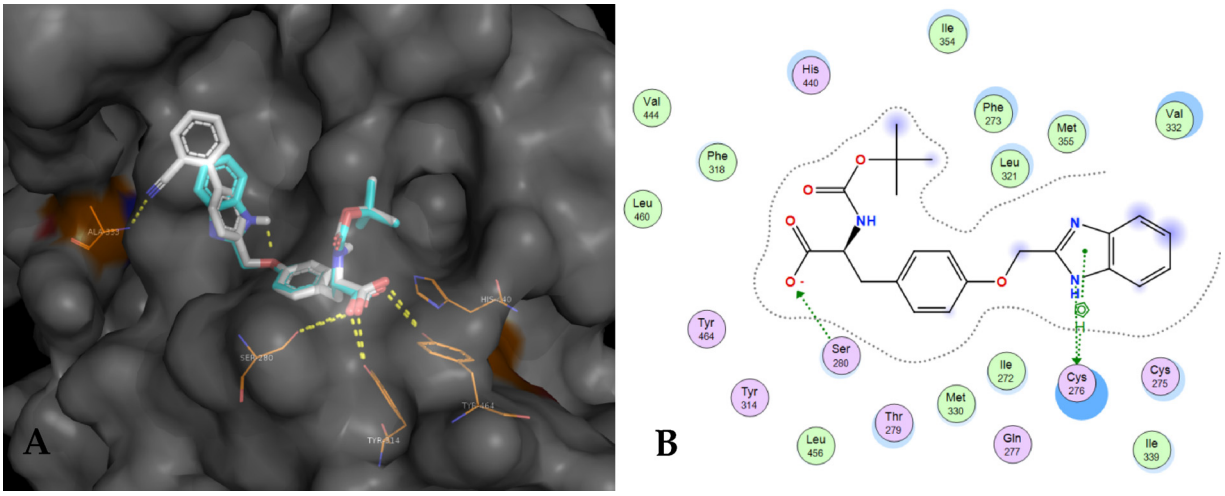

Fig. 8. (A) 3-D binding diagram of compounds **1** and **3** in the PPARα ligand binding pocket. The stick models represent: **1** (cyan), **3** (white), and amino acids as orange lines. Yellow lines suggest polar contacts. (B) 2-D interaction map for compound **1** on PPARα.

results obtained in the antidiabetic assay. Fig. 7 shows the results of these assessments; compound **1** (100 mg/kg) significantly reduced blood glucose 60 min after glucose load (2 g/kg) compared with the vehicle group, which presented the maximum blood glucose level at this time. An area under the curve (AUC) graph confirmed the efficacy of **1**, which significantly decreased the AUC by approximately 25% (p = 0.05). During the experiment, glucose levels did not decrease beyond baseline, indicating that the antidiabetic action of compound **1** is due to an antihyperglycemic effect rather than a hypoglycemic effect in agreement with PTP-1B inhibition and PPAR activation related to insulin sensitization. Compound **3** showed lack of activity in OGTT.

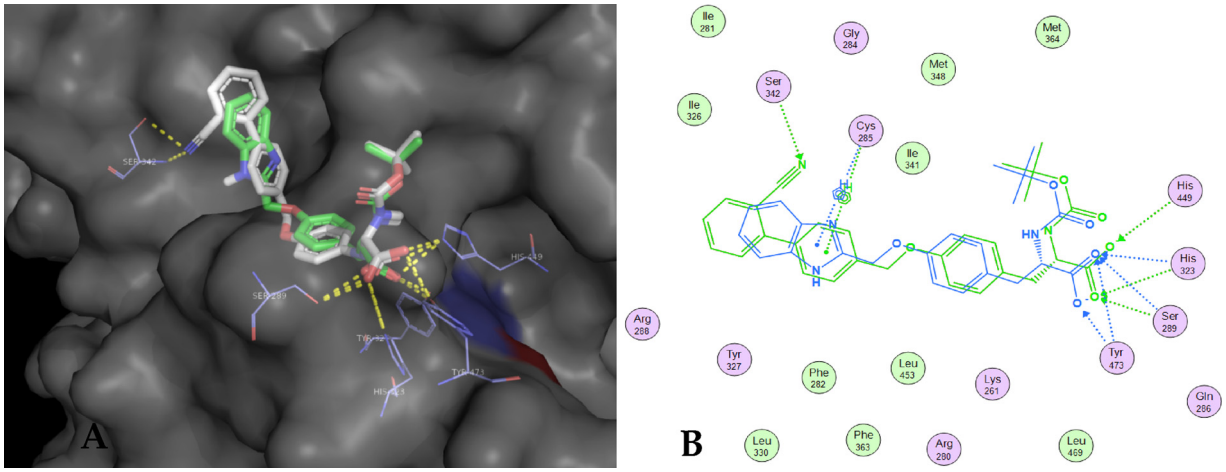

Fig. 9. (A) 3-D binding diagram of **1** and **3** into the into the PPARγ ligand binding pocket. The stick models represent: **1** (green), **3** (white), and amino acids as cyan lines. Yellow lines suggest polar contacts. (B) 2-D overlay map for **1** and **3** on PPARγ.

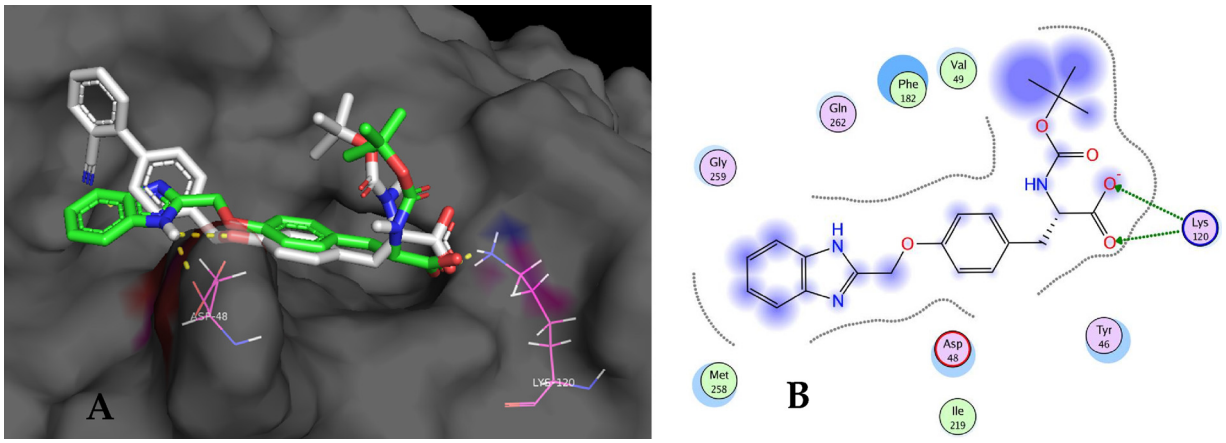

Fig. 10. (A) Binding diagram of **1** and **3** into the active site of PTP-1B. The stick models represent: **1** (green), **3** (white), and amino acids as magenta lines. Yellow lines suggest polar contacts. (B) 2-D interaction map for **1** on PTP-1B.

Table 1
Molecular docking binding energies for compounds **1** and **3** and their multi-targets.

Compound	PPAR-α ΔG (Kcal/mol)	PPAR-γ ΔG (Kcal/mol)	PTP-1B ΔG (Kcal/mol)
1	−8.2	−9.6	−7.1
3	−9.9	−10.7	−6.5

3.5. Molecular docking calculation

Based on the *in vitro* and *in vivo* biological results, the most potent compounds, **1** and **3,** were designated to elucidate the experimental effects on relevant T2DM protein targets. A pilot molecular docking calculation was performed employing DIA-DB [2,32], a European web server, for the prediction of antidiabetic compounds using inverse virtual screening of the molecules **1–5** *versus* a set of eighteen different targets recognized as crucial proteins in T2DM, including PPARα, PPARγ and PTP-1B, *inter alia* [33]. Afterward, a more precise and refined study was conducted for the most attractive compounds (**1** and **3**). Refined docking calculation revealed that molecules **1** and **3** go into the ligand binding pocket of PPARα and generate a network of ionic and hydrogen bonds with Ser-280, Tyr-314, Tyr-464 and His-440, critical amino acids for the activation of this nuclear receptor. Compound **1**, which was the most potent in the *in vitro* assay, showed two extra interactions with Cys-276; one of them was a type π−H interaction, and the other one was a polar interaction. Compound **3** also showed an extra interaction with Ala-333 (Fig. 8).

Compounds **1** and **3** adopt a conformation inside the PPARγ ligand binding pocket and connect by means of ionic and hydrogen bonds with His-449, His-323, Tyr-473 and Ser-289, critical amino acids for the activation of PPARγ (Fig. 9).

The most active compound (**3**) *in vitro* displayed an extra interaction with Ser-342 (Fig. 9), distinguishing of PPARγ partial agonists. Glitazones, which are full PPARγ agonists, shows side effects such as weight gain and congestive heart failure, among other undesired effects. However, partial agonists are not related to these adverse effects [34].

In the case of PTP-1B, binding postures represented in Fig. 10 suggest that **1** and **3** do not internalize in the catalytic pocket of PTP-1B; both interact *via* ionic bonds with the residue Lys-120 in the surface of this pocket [35]. Compound **1** showed an additional interaction with Asp-48. This could be the reason why both compounds showed IC_{50}s of approximately 44 μM against PTP-1B.

Molecular docking scores (binding energies) are reported in Table 1 for compounds **1** and **3**, and their polypharmacological targets.

Both binding energies and ligand-induced interactions correlate with the behavior of compounds **1** and **3** in the *in vitro* assays, suggesting that computational tools are useful in drug discovery.

4. Conclusion

In summary, five *N*-Boc-L-tyrosine derivatives have been developed

as new chemical entities for the treatment of type 2 diabetes mellitus. Compounds **1** and **3** (a) significantly increased the mRNA expression of PPARα, PPARγ, FATP-1 and GLUT-4 to a greater extent than fenofibrate and pioglitazone, (b) inhibited PTP-1B activity, (c) showed polypharmacological (multitargeting) profiles based on the *in vitro* and *in silico* experiments, and (d) decreased glucose levels *in vivo* with antihyperglycemic effects related to insulin sensitization mechanisms.

Conflict of interests

The authors declared that there is no conflict of interests regarding the publication of this paper.

Acknowledgements

This work has been supported by CONACyT (Consejo Nacional de Ciencia y Tecnología from Mexico) under Grant # 253814 (Ciencia Básica, 2015) given to G. Navarrete-Vazquez. M. A. Herrera-Rueda received a CONACYT support (483277) in order to reach Doctoral studies. The authors thank CIQ-LANEM Laboratory for structural analysis. We also thank the Facultad de Farmacia and Centro de Investigaciones Químicas, UAEM for providing some research supplies for this study.

References

[1] N. Li, L.J. Wang, B. Jiang, X.Q. Li, C.L. Guo, S.J. Guo, D.Y. Shi, Recent progress of the development of dipeptidyl peptidase-4 inhibitors for the treatment of type 2 diabetes mellitus, Eur. J. Med. Chem. 151 (2018) 145–157.

[2] B. Colín-Lozano, S. Estrada-Soto, F. Chávez-Silva, A. Gutiérrez-Hernández, L. Cerón-Romero, A. Giacoman-Martínez, J.C. Almanza-Pérez, E. Hernández-Núñez, Z. Wang, X. Xie, M. Cappiello, F. Balestri, U. Mura, G. Navarrete-Vazquez, Design, synthesis and in combo antidiabetic bioevaluation of multitarget phenylpropanoic acids, Molecules 23 (2018) 340.

[3] A. Mooradian, Dyslipidemia in type 2 diabetes mellitus, Nat. Clin. Pract. Endocrinol. Metab. 5 (2009) 150–159.

[4] A. de Souza Bastos, D.T. Graves, A.P. de Melo Loureiro, C.R. Júnior, S.C.T. Corbi, F. Frizzera, R.M. Scarel-Caminaga, N.O. Câmara, O.M. Andriankaja, M.I. Hiyane, S.R.P. Orrico, Diabetes and increased lipid peroxidation are associated with systemic inflammation even in well-controlled patients, J. Diab. Complications 30 (2016) 1593–1599.

[5] A. Ceriello, A. Quatraro, D. Giugliano, Diabetes mellitus and hypertension: the possible role of hyperglycemia through oxidative stress, Diabetologia 36 (1993) 265–266.

[6] Q. Chen, Y. Zhang, D. Ding, D. Li, M. Xia, X. Li, Y. Yang, Q. Li, G. Hu, W. Ling, Metabolic syndrome and its individual components with mortality among patients with coronary heart disease, Int. J. Cardiol. 224 (2016) 8–14.

[7] G. Navarrete-Vázquez, H. Torres-Gómez, S. Hidalgo-Figueroa, J.J. Ramírez-Espinosa, S. Estrada-Soto, J.L. Medina-Franco, I. León-Rivera, F.J. Alarcón-Aguilar, J.C. Almanza-Pérez, Synthesis, in vitro and in silico studies of a PPARγ and GLUT-4 modulator with hypoglycemic effect, Bioorg. Med. Chem. Lett. 24 (2014) 4575–4579.

[8] Q. Wu, A.M. Ortegon, B. Tsang, H. Doege, K.R. Feingold, A. Stahl, FATP1 is an insulin-sensitive fatty acid transporter involved in diet-induced obesity, Mol. Cell. Biol. 26 (2006) 3455–3467.

[9] P. Balakumar, M. Rose, S.S. Ganti, P. Krishan, M. Singh, PPAR dual agonists: are they opening pandora's box? Pharmacol. Res. 56 (2007) 91–98.

[10] Y. Wang, J. Liu, P.J. Dransfield, L. Zhu, Z. Wang, X. Du, X. Jiao, Y. Su, A.R. Li, S.P. Brown, A. Kasparian, M. Vimolratana, M. Yu, V. Pattaropong, J.B. Houze, G. Swaminath, T. Tran, K. Nguyen, Q. Guo, J. Zhang, F. Li, L. Zhuang, M.D. Miao, T.L. Bartberger, D. Correll, S. Chow, J. Wong, Luo, D.C.H. Lin, J.C. Medina, Discovery and optimization of potent GPR40 full agonists containing tricyclic spirocycles, ACS Med. Chem. Lett. 4 (2013) 551–555.

[11] M. Parimala, M. Debjani, H.R. Vasanthi, F.G. Shoba, F. Nymphaea Burm, Hydroalcoholic seed extract increases glucose consumption in 3T3-L1 adipocytes through activation of peroxisome proliferator-activated receptor gamma and insulin sensitization, J. Adv. Pharm. Technol. Res. 6 (2015) 183.

[12] Y. Fujiwara, C. Tsukahara, N. Ikeda, Y. Sone, T. Ishikawa, I. Ichi, T. Koike, Y. Aoki, Oleuropein improves insulin resistance in skeletal muscle by promoting the translocation of GLUT4, J. Clin. Biochem. Nutr. 61 (2017) 196–202.

[13] B.G. Shearer, A.N. Billin, The next generation of PPAR drugs: do we have the tools to find them? Biochim. Biophys. Acta - Mol. Cell Biol. Lipids 1771 (2007) 1082–1093.

[14] B.R. Henke, Peroxisome proliferator-activated receptor Alpha/gamma dual agonists for the treatment of type 2 diabetes, J. Med. Chem. 47 (2004) 4118–4127.

[15] B.K. He, Z.Q. Ning, Z.B. Li, S. Shan, D.S. Pan, B.C. Ko, P.P. Li, Z.F. Shen, G.F. Dou, B.L. Zhang, X.P. Lu, Y. Gao, in vitro and in vivo characterizations of chiglitazar, a newly identified PPAR pan-agonist, PPAR Res. 2012 (2012) 546548.

[16] A. Rubenstrunk, R. Hanf, D.W. Hum, J.C. Fruchart, B. Staels, Safety issues and prospects for future generations of PPAR modulators, Biochim. Biophys. Acta - Mol. Cell Biol. Lipids 1771 (2007) 1065–1081.

[17] G. Navarrete-Vazquez, P. Paoli, I. León-Rivera, R. Villalobos-Molina, J.L. Medina-Franco, R. Ortiz-Andrade, S. Estrada-Soto, G. Camici, D. Diaz-Coutiño, I. Gallardo-Ortiz, K. Martinez-Mayorga, H. Moreno-Díaz, Synthesis, in vitro and computational studies of protein tyrosine phosphatase 1B inhibition of a small library of 2-arylsulfonylaminobenzothiazoles with antihyperglycemic activity, Bioorg. Med. Chem. 17 (2009) 3332–3341.

[18] G. Navarrete-Vazquez, M. Ramírez-Martínez, S. Estrada-Soto, C. Nava-Zuazo, P. Paoli, G. Camici, J. Escalante-García, J.L. Medina-Franco, F. López-Vallejo, R. Ortiz-Andrade, Synthesis, in vitro and in silico screening of ethyl 2-(6-substituted benzo[d]thiazol-2-ylamino)-2-oxoacetates as protein-tyrosine phosphatase 1B inhibitors, Eur. J. Med. Chem. 53 (2012) 346–355.

[19] L. Cerón-Romero, P. Paoli, G. Camici, V. Flores-Morales, M.Y. Rios, J.J. Ramírez-Espinosa, S. Hidalgo-Figueroa, G. Navarrete-Vázquez, S. Estrada-Soto, In vitro and in silico PTP-1B inhibition and in vivo antidiabetic activity of semisynthetic moronic acid derivatives, Bioorg. Med. Chem. Lett. 26 (2016) 2018–2022.

[20] G. Navarrete-Vázquez, M.G. Morales-Vilchis, S. Estrada-Soto, J.J. Ramírez-Espinosa, S. Hidalgo-Figueroa, C. Nava-Zuazo, H. Tlahuext, I. Leon-Rivera, J.L. Medina-Franco, F. López-Vallejo, S.P. Webster, M. Binnie, R. Ortiz-Andrade, H. Moreno-Diaz, Synthesis of 2-{2-[(α/β-naphthalen-1-ylsulfonyl)amino]-1,3-thiazol-4-yl}acetamides with 11β-hydroxysteroid dehydrogenase inhibition and in combo antidiabetic activities, Eur. J. Med. Chem. 74 (2014) 179–186.

[21] B. Filippis, P. Linciano, A. Ammazzalorso, C. Giovanni, M. Fantacuzzi, L. Giampietro, A. Laghezza, C. Maccallini, P. Tortorella, A. Lavecchia, F. Loiodice, R. Amoroso, Structural development studies of PPARs ligands based on tyrosine scaffold, Eur. J. Med. Chem. 89 (2015) 817–825.

[22] N. Thangavel, M. Al Bratty, S. Akhtar Javed, W. Ahsan, H.A. Alhazmi, Targeting peroxisome proliferator-activated receptors using thiazolidinediones: strategy for design of novel antidiabetic drugs, Int. J. Med. Chem. 2017 (2017) 1–20.

[23] B.R. Bhattarai, B. Kafle, J.S. Hwang, S.W. Ham, K.H. Lee, H. Park, I.O. Han, H. Cho, Novel thiazolidinedione derivatives with anti-obesity effects: dual action as PTP-1B inhibitors and PPAR-γ activators, Bioorg. Med. Chem. Lett. 20 (2010) 6758–6763.

[24] P. Paoli, A. Modesti, F. Magherini, T. Gamberi, A. Caselli, G. Manao, G. Raugei, G. Camici, G. Ramponi, Site-directed mutagenesis of two aromatic residues lining the active site pocket of the yeast Ltp1, Biochim. Biophys. Acta 1770 (2007) 753–762.

[25] S. Hidalgo-Figueroa, J.J. Ramírez-Espinosa, S. Estrada-Soto, J.C. Almanza-Pérez, R. Román-Ramos, J.F. Alarcón-Aguilar, J.V. Hernández-Rosado, H. Moreno-Díaz, D. Díaz-Coutiño, G. Navarrete-Vázquez, Discovery of thiazolidine-2,4-dione/biphenylcarbonitrile hybrid as dual PPAR α/γ modulator with antidiabetic effect: in vitro, in silico and in vivo approaches, Chem. Biol. Drug Des. 81 (2013) 474–483.

[26] R. García-Macedo, F. Sánchez-Muñoz, J.C. Almanza-Pérez, G. Duran-Reyes, F. Alarcón-Aguilar, M. Cruz, Glycine increases mRNA adiponectin and diminishes pro-inflammatory adipokines expression in 3T3-L1 cells, Eur. J. Pharmacol. 587 (2008) 317–321.

[27] J.C. Almanza-Pérez, F.J. Alarcón-Aguilar, G. Blancas- Flores, A.E. Campos-Sepúlveda, R. Román-Ramos, R. García-Macedo, M. Cruz, Glycine regulates inflammatory markers modifying the energetic balance through PPAR and UCP-2, Biomed. Pharmacother. 64 (2010) 534–540.

[28] S. Hidalgo-Figueroa, G. Navarrete-Vázquez, S. Estrada-Soto, D. Giles-Rivas, F.J. Alarcón-Aguilar, I. León-Rivera, A. Giacoman-Martínez, E. Miranda Pérez, J.C. Almanza-Pérez, Discovery of new dual PPARγ-GPR40 agonists with robust antidiabetic activity: design, synthesis and in combo drug evaluation, Biomed. Pharmacother. 90 (2017) 53–61.

[29] E. Gutierrez-Lara, C. Martínez-Conde, E. Rosales-Ortega, J.J. Ramírez-Espinosa, J.C. Rivera-Leyva, D. Centurión, K. Carvajal, D. Ortega-Cuellar, S. Estrada-Soto, G. Navarrete-Vázquez, Synthesis and in vitro AMPK activation of cycloalkyl/alkarylbiguanides with robust in vivo antihyperglycemic action, J. Chem. 1212609 (2017) 1–8.

[30] Molecular Operating Environment (MOE), 2018.01, Chemical Computing Group ULC, 1010 Sherbooke St. West, Site #910, Montreal, QC, Canada, H3A 2R7, 2018http://www.chemcomp.com.

[31] O. Méndez-Lucio, J. Naveja, H. Vite-Caritino, F. Prieto-Martínez, J. Medina-Franco, Polypharmacology in drug Discovery, in: N. Handler (Ed.), Drug Selectivity. An Evolving Concept in Medicinal Chemistry, Wiley, 2017, pp. 1–29.

[32] http://bio-hpc.ucam.edu/dia-db/.

[33] A. Sánchez-Pérez, A. Muñoz, J. Peña-García, H. den-Haan, N. Bekas, A. Katsikoudi, A.G. Tzakos, H. Pérez-Sánchez, DIA-DB: a web-accessible database for the prediction of diabetes drugs, Bioinform. Biomed. Eng. 9044 (2015) 655–663.

[34] D. Capelli, C. Cerchia, R. Montanari, F. Loiodice, P. Tortorella, A. Laghezza, L. Cervoni, G. Pochetti, A. Lavecchia, Structural basis for PPAR partial or full activation revealed by a novel ligand binding mode, Sci. Rep. 6 (2016) 34792.

[35] S. Hidalgo-Figueroa, S. Estrada-Soto, J.J. Ramírez-Espinosa, P. Paoli, G. Lori, I. León-Rivera, G. Navarrete-Vázquez, Synthesis and evaluation of thiazolidine-2,4-dione/benzazole derivatives as inhibitors of protein tyrosine phosphatase 1B (PTP-1B): antihyperglycemic activity with molecular docking study, Biomed. Pharmacother. 107 (2018) 1302–1310.